EPR and optical spectroscopy of structural phase transition in a Rb_2NaYF_6 crystal

M. L. Falin,[1,2] K. I. Gerasimov,[1,2] V. A. Latypov,[1] A. M. Leushin,[2] and N. M. Khaidukov[3]
[1]*Kazan Zavoisky Physical-Technical Institute, Russian Academy of Sciences, 420029 Kazan, Russian Federation*
[2]*Kazan (Volga Region) Federal University, Kazan 420008, Russian Federation*
[3]*Institute of General and Inorganic Chemistry, Russian Academy of Sciences, Moscow 119991, Russian Federation*
(Received 30 November 2012; revised manuscript received 27 February 2013; published 28 March 2013)

The structural phase transition has been observed for the first time in the Rb_2NaYF_6 crystal and studied by EPR and optical spectroscopy. EPR spectra of Dy^{3+} and Yb^{3+} ions present as unintentional dopants in the nominally undoped crystal and forming tetragonal paramagnetic centers have been identified. A characteristic splitting of some optical lines has been observed in the temperature dependence of the Yb^{3+} optical spectra. It indicates the splitting of the cubic quartet energy levels of Yb^{3+} ions by the tetragonal crystal field. The empirical schemes of the energy levels for cubic and tetragonal paramagnetic centers of Yb^{3+} ions have been established and parameters of the corresponding crystal fields have been determined. The latter have been used for analyzing the crystal lattice distortions occurring in the vicinity of the Yb^{3+} ion during the phase transition. It has been established using the superposition model that the nearest octahedral environment of the Yb^{3+} ion is distorted as follows: the fluorine ions are rotated by the angle of 2.1° around the fourfold axis; the F^- ions located symmetrically in the plane perpendicular to the rotation axis approach the dopant by 0.0014 nm, whereas the F^- ions located on the rotation axis move away by 0.0028 nm. It has been concluded that the studied phase transition includes the critical rotations of the octahedral F groups and noncritical displacement of atoms in the rotated fluorine octahedra.

DOI: 10.1103/PhysRevB.87.115145 PACS number(s): 76.30.Kg, 61.72.Bb, 78.60.Lc, 64.60.Bd

I. INTRODUCTION

Hexahalide compounds with the general formula $A_2B\mathrm{Ln}X_6$, where A and B are monovalent alkali metal ions, X is a halide anion, and Ln^{3+} is a trivalent rare-earth or Y cation, exhibit the cubic elpasolite structure with the space group $Fm\bar{3}m(O_h^5)$ over a wide temperature range.[1–3] The structural arrangement corresponds to that of a perovskite with an additional cationic ordering in the octahedral sites. Trivalent cations (Ln^{3+}) and smaller monovalent cations (B^+) are located in the octahedral 4a and 4b sites, respectively, where the larger monovalent cations (A^+) are located in the 8c sites and are surrounded by twelve anions, which form a cuboctahedron. The crystal structure is then a three-dimensional network of corner-sharing BF_6 and LnF_6 octahedra with the A cations sitting at the center of a cube formed by eight octahedra.

The fact that lanthanide elpasolites are the most symmetric crystal systems available for Ln^{3+} makes them model systems for understanding static and dynamic processes in solid state. In addition, the $A_2B\mathrm{Ln}X_6$ system exists for the series La^{3+} ($4f^0$) to Lu^{3+} ($4f^{14}$), including Y^{3+}, and thus provides the possibility of systematic studies. Therefore the magnetic properties of various elpasolite rare-earth fluorides[4] and energy transfer phenomena[5] were intensively studied. A large number of studies concerned electronic spectra of pure $A_2B\mathrm{Ln}X_6$ and doped $A_2B\mathrm{Y}X_6$: Ln^{3+} systems. To obtain information about highly degenerate electronic energy levels of Ln^{3+} in $\mathrm{Ln}X_6^{3-}$ complexes,[6–13] optical spectra of Ln^{3+} have been always interpreted in terms of the octahedral (O_h) crystal field (CF). The effects observed in some $A_2B\mathrm{Ln}X_6$ systems at low temperatures,[6,13] due to the lowering of the CF symmetry to C_{4h}, were considered to be small and not taken into account.

The elpasolite crystals are model systems for studying mechanisms of phase transitions.[14] It is well known that elpasolite-like related materials with corner-linked octahedra such as perovskites or cryolite compounds tend to be unstable especially against collective tilts of octahedra.[2,3,15–17] The point is that in the hard-sphere model of an ionic contact, it is necessary to simultaneously satisfy the conditions $r_{A^+} + r_{X^-} = a\sqrt{2}/4$ and $2r_{X^-} + r_{B^+} + r_{\mathrm{Ln}^{3+}} = a/2$, where $r_{A^+}, r_{X^+}, r_{B^+}, r_{\mathrm{Ln}^{3+}}$ are the ionic radii of the corresponding ions and a is the lattice parameter. These requirements are combined in the so-called "Goldshmidt tolerance factor" $t_G = \sqrt{2}(r_{A^+} + r_{F^-})/(2r_{F^-} + r_{B^+} + r_{M^{3+}})$,[18] which, in the ideal case, is unity. In reality, elpasolite-structured compounds adopt the cubic arrangement for $0.88 \leqslant t_G \leqslant 1.0$. The occurrence of the structural phase transition depends mainly on factors: 1) the electronic structure of the rear-earth (RE) ion, i.e., the presence of a Jahn-Teller configuration, or 2) the t_G value being close to the lower boundary of the stability range. Phase transitions, involving the cooperative Jahn-Teller distortion of elpasolite-structured compounds, occur at very low temperature.[19] For the structural phase transition with lower t_G values, there are a number of possibilities, including a correlated tilting of the $\mathrm{Ln}X_6$ and $\mathrm{B}X_6$ octahedra, distortions of the octahedral units, and cooperative displacements of the A cations away from the centers of cuboctahedra. Usually the structural distortions are associated with rotations of the octahedra yielding a tetragonal phase (space group $I4/m{-}C_{4h}^5$). These distortions are associated with the combination of octahedral rotations and ion displacements in the tetragonal phase yielding a monoclinic phase ($P12_1/n1$).

Systematic studies of the nature of the structural distortions within fluoroelpasolite have largely concentrated on Rb_2KLnF_6, Rb_2NaLnF_6, Cs_2KLnF_6, Cs_2NaLnF_6, Cs_2RbLnF_6 type of compounds, since these are numerous and relevant from the technological point of view. One or several phase transitions have been observed in most of fluoroelpasolities between 130 and 480 K and have been investigated using various techniques, e.g., x-ray diffraction,[16,20–22] NMR,[23,24] EPR,[25,26]

heat capacity measurements,[27] Raman scattering,[28] and hydrostatic pressure.[29,30] Fluoroelpasolites have a wide range of combinations of the A_2B atoms leading to various transition options; single: $Fm\bar{3}m(O_h^5) \rightarrow I4/m(C_{4h}^5)$ (Rb_2Na, Cs_2K; at values $t_G > 0.915$), double: $Fm\bar{3}m(O_h^5) \rightarrow I4/m(C_{4h}^5) \rightarrow P2_1/n(C_{2h}^5)$ (Rb_2K), or triple: $Fm\bar{3}m \rightarrow I4/m \rightarrow I2/m \rightarrow P2_1/n$ (Cs_2Rb; at values $0.901 > t_G > 0.880$), and also trigger transitions $Fm\bar{3}m \rightarrow P2_1/n$ (Rb_2K; at values $t_G < 0.872$).[31] Usually, single phase transitions in these structures are connected with the lattice instability with respect to the critical rotations of the octahedral LnF_6 ions due to the condensation of soft phonon modes. However, to explain such transitions, it is necessary to take into account noncritical displacements of atoms, which are reduced due to slight distortions of octahedra and displacements of the A atoms located in the inter-octahedral voids.[32]

In the most studied crystals, a RE^{3+} ion is in the center of the LnF_6 octahedron. To the best of our knowledge, there are only two works,[33,34] where Y^{3+} serves as Ln^{3+} (Rb_2KYF_6). The substitution of the RE^{3+} ion for the Y^{3+} ion does not alter the general picture of the phase transitions inherent to the series of fluoroelpasolites with the atomic combination Rb_2K. No phase transitions were observed in the Rb_2NaYF_6 crystal.[1,2,4,10,35–37] It was assumed that this crystal has the elpasolite structure $Fm3m$.

This work presents the results of the electron paramagnetic resonance (EPR) and optical spectroscopy study indicating the first observation of the structural phase transition in the Rb_2NaYF_6 crystal (with $t_G = 0.921$) containing the Y^{3+} ion as the Ln^{3+}. It is organized as follows. In Sec. II, the experimental results are presented. In Sec. III, the empirical schemes of the energy levels for cubic and tetragonal paramagnetic centers of Yb^{3+} ions and CF parameters (CFPs) are determined. These CFPs are used to analyze the phase transitions based on the superposition model and to determine the structure of the nearest environment of theYb^{3+} ion.

II. EXPERIMENTAL RESULTS

Undoped Rb_2NaYF_6 crystals were grown under hydrothermal conditions using autoclaves with copper inserts having a volume of about 40 cm^3 and the inserts were separated by perforated diaphragms into synthesis and crystallization zones. The fluoride crystals were synthesized by a direct temperature-gradient method as a result of the reaction of the aqueous solutions containing 35–40 mol% RbF and 8–10 mol% NaF with Y_2O_3 at a temperature of about 750 K in the synthesis zone, a temperature gradient along the reactor body of up to 3 K/cm, and a pressure of about 100 MPa. Under these conditions, spontaneously nucleated crystals up to 0.5 cm^3 in size were grown in the upper crystallization zone of the autoclave for 200 hours. The purities of the utilized Y_2O_3 oxides were 99.9% (sample I) and 99.999% (sample II), respectively. The structure type, stoichiometry, and phase purity of synthesized samples were characterized by powder x-ray diffraction at room temperature. Rare-earth impurity ions in crystals, synthesized with 99.9% Y_2O_3 as the raw material, were identified by optical and EPR spectroscopy.

EPR experiments were carried out on a modified ERS-231 (Germany) spectrometer working in the X band (9.5 GHz)[38] at the temperatures of 4.2 and 7–300 K. Optical spectra were recorded on a homebuilt multifunctional spectrometer[39] at $T =$ 2 and 4.2 K using an optical helium cryostat. To measure EPR and optical spectra at the temperatures of 7–300 K, we used a helium gas flow cryostat CRYO202ESR (Chernogolovka, Russia). A semiconductor laser diode ATC-C1000-100-TMF-965 (St. Petersburg, Russia) of the power of 1 W was used as a source of a laser selective excitation with the laser linewidth on the order of 2 nm. The emission output wavelength was tunable from 963 nm (10 381 cm^{-1}) to 969 nm (10 317 cm^{-1}). A cooled photomultiplier was used as a detector.

Intense lines are observed in EPR spectra of the Rb_2NaYF_6 crystal (samples I and II) in a wide temperature interval (4.2–300 K) due to the intrinsic paramagnetic centers, i.e., "growth" centers formed in all fluoride elpasolites (hexafluoroelpasolite) synthesized by the hydrothermal method: Cs_2NaYF_6, Cs_2NaScF_6, Cs_2NaGaF_6, Cs2NaLuF6, and Cs_2KYF_6. Additional paramagnetic centers are also observed in the sample I at the temperatures of 4.2–40 K. Their comparative analysis indicates that they are formed by the Dy^{3+} and Yb^{3+} ions (see Fig. 1), which are present as unintentional impurities in the crystal. It was established from the angular dependencies of the EPR lines in the (001) plane that the Dy^{3+} and Yb^{3+} paramagnetic centers forms three magnetically inequivalent complexes of tetragonal symmetry (T_{tet} in Fig. 2). The tetragonal EPR spectra fit the spin Hamiltonian (SH)

$$\mathscr{H} = g_{||}\beta H_z S_z + g_{\perp}\beta(H_x S_x + H_y S_y) + A_{||} S_z I_z + A_{\perp}(S_x I_x + S_y I_y),$$

where $S = 1/2$, ^{even}I (Dy,Yb) $= 0$, $^{161,163}I$ (Dy) $= 5/2$, ^{171}I (Yb) $= 1/2$, ^{173}I (Yb) $= 7/2$, A is the hyperfine interaction constant, the Z, X, and Y axes are parallel to the crystallographic [100], [010], and [001] axes, respectively.

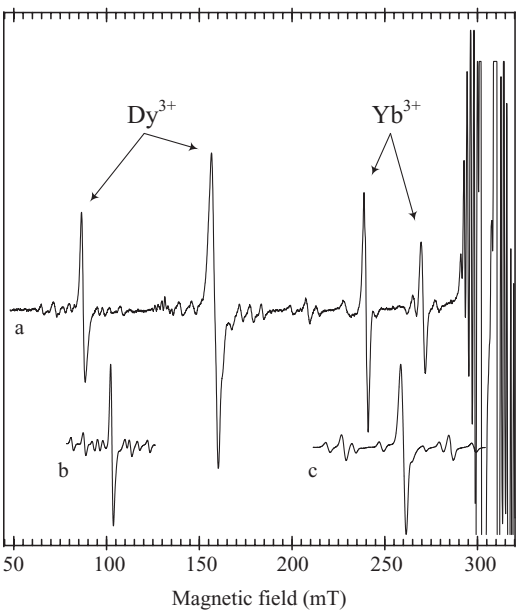

FIG. 1. EPR spectra of (a) Dy^{3+} and Yb^{3+} ions in the Rb_2NaYF_6 crystal, (b) Dy^{3+} ion (T_c - cubic) in the $KZnF_3$ and (c) Yb^{3+} ion (T_c) in the Cs_2NaYF_6 crystal at $T = 7$ K for H ∥ [100] and $\nu = 9360.7$ MHz.

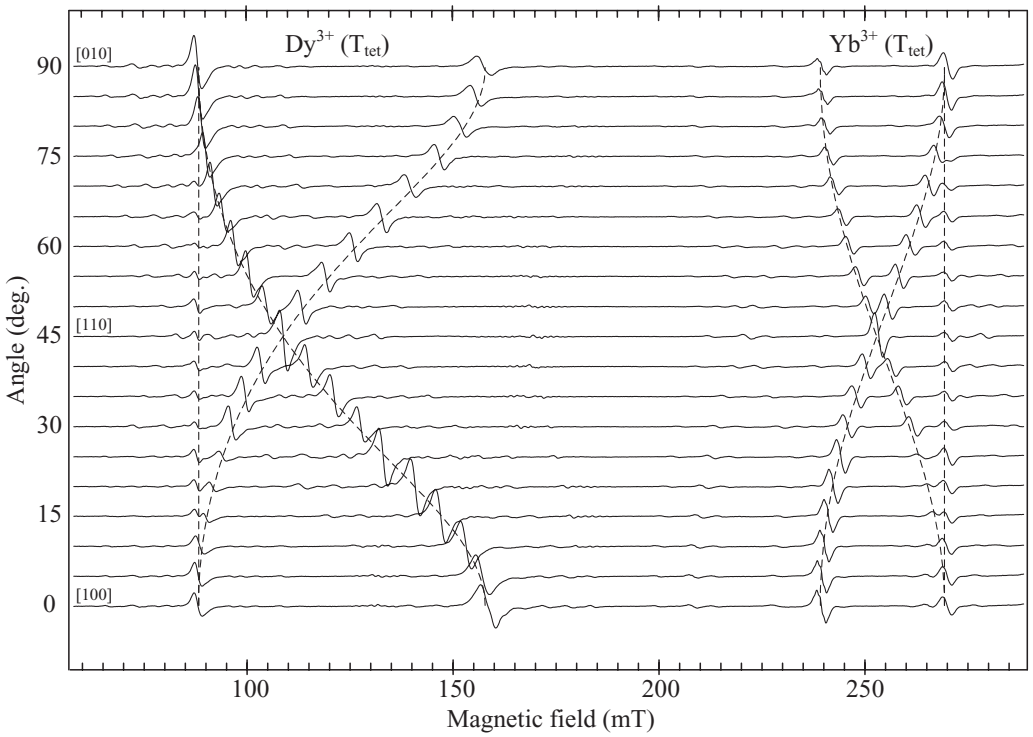

FIG. 2. Angular dependencies of EPR spectra of Dy^{3+} (T_{tet}) and Yb^{3+} (T_{tet}) ions in the Rb_2NaYF_6 crystal at $T = 7$ K and the rotation of the magnetic field H in the (001) plane and $\nu = 9360.7$ MHz, theory with the SH parameters from Table I.

Least-squares fit SH parameters were calculated by computer using an iterative procedure which included complete diagonalization of the SH. The results are given in Table I.

In the crystal with cubic symmetry, where the isovalent substitution (the trivalent impurity ion substitutes Y^{3+} ion) is implemented, tetragonal complexes are formed. A question arises if the Cs_2NaYF_6 crystal is cubic. Up to now, numerous studies of this crystal did not reveal any deviations from "cubicity."[1,2,4,10,35,37] The temperature dependence of the EPR spectra of Dy^{3+} and Yb^{3+} (see Fig. 3) also did not show any transformations in the crystal lattice in the whole temperature range. The origin of tetragonal complexes remains unclear. However, the structure and linewidth of the EPR spectrum of the "growth" center (see Figs. 4 and 5) sharply change between $T = 155$ and 4.2 K, which may indicate the presence of the phase transition at 150 ± 2 K. The origin of this phase transition may be twofold: either due to admixture paramagnetic ions or it is inherent to the pure crystal. The temperature behavior of EPR spectra of the "growth" center of the nominally pure Rb_2NaYF_6 crystal (sample II) (see Fig. 6), where the RE^{3+} impurity ions are not observed, confirms that the crystal undergoes a phase transition.

EPR spectra of Dy^{3+} and Yb^{3+} ions are observed in the narrow temperature range from 40 to 4.2 K. To study the phase transition at 150 K, we used the optical spectroscopy of Yb^{3+} ions. Luminescence spectra of Yb^{3+} at the temperatures of 2, 77, and 160 K are shown in Fig. 7. The spectral lines are interpreted as the electronic transitions due to Yb^{3+} at the T_c and T_{tet} centers, yielding the energy levels shown in Fig. 8(b). The luminescence lines of Yb^{3+} (T_c) in Rb_2NaYF_6 corresponding to the electronic transitions from the $^2\Gamma_8$ level to the sublevels of the $^2F_{7/2}$ multiplet were chosen analogous to those of Yb^{3+} in Cs_2NaYF_6.[12] The line at 10 395 cm^{-1} and $T = 160$ K, observed both in the excitation and luminescence

TABLE I. Values of g factors and hyperfine interaction constant A (in 10^{-4} cm^{-1}) for Dy^{3+} and Yb^{3+} ions in Rb_2NaYF_6; corresponding parameters for RE^{3+}: Cs_2NaYF_6 and $KZnF_3$ are given for comparison.

Crystal	Ion	Symmetry	$g_\parallel$	$g_\perp$	$A_\parallel$	$A_\perp$	
Rb_2NaYF_6	$^{161}Dy^{3+}$	Tetragonal	4.183 (5)	7.640 (5)	129.8 (8)	216.4 (8)	Present work
$a_o = 0.88693$ nm[1]	$^{163}Dy^{3+}$				300.8 (8)	236.8 (8)	
	$^{171}Yb^{3+}$		2.788 (5)	2.473 (5)	739.9 (8)	656.5 (8)	
	$^{173}Yb^{3+}$				203.1 (8)	182.5 (8)	
Cs_2NaYF_6	$^{171}Yb^{3+}$	Cubic	2.588		686.1		Ref. 41
$a_o = 0.9056$ nm	$^{173}Yb^{3+}$				189.1		
$KZnF_3$	$^{161}Dy^{3+}$		6.551		186.3		Ref. 40
$a_o = 0.4046$ nm	$^{163}Dy^{3+}$				252.6		

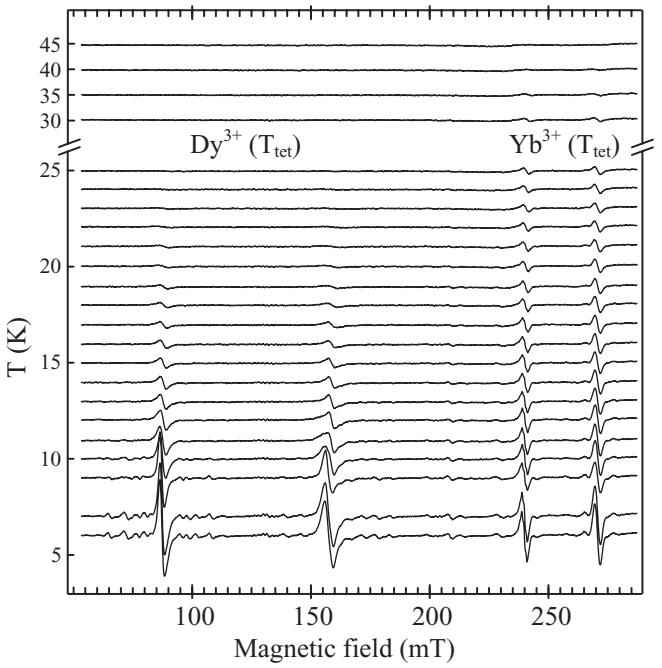

FIG. 3. Temperature dependence of EPR spectra of Dy^{3+} and Yb^{3+} in the Rb_2NaYF_6 crystal for H ∥ [100] and $\nu = 9360.7$ MHz.

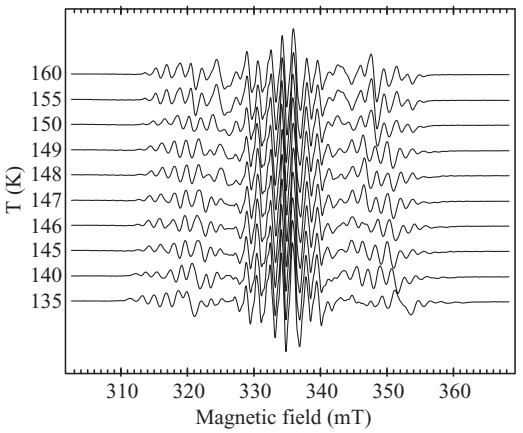

FIG. 5. Fragment of EPR spectra of the "growth" center in the Rb_2NaYF_6 crystal (sample I) near the phase transition temperature for H ∥ [100] and $\nu = 9360.7$ MHz.

spectrum, is assigned to the $^2\Gamma_8 \leftrightarrow {}^1\Gamma_6$ (T_c) transition. The luminescence lines at the temperatures 4.2–150 K are shown in Fig. 8(a). They correspond to the electronic transitions $^2\Gamma_8 \rightarrow {}^1\Gamma_6$ (1_c) for Yb^{3+} (T_c) and $^3\Gamma_{t7} \rightarrow {}^1\Gamma_{t6}$ (1_t), $^3\Gamma_{t6} \rightarrow {}^1\Gamma_{t6}$ (2_t) for Yb^{3+} (T_{tet}) at the temperatures below 150 K. The luminescence line splits into two components with lowering temperature. This splitting may be explained by the removal of the fourfold degeneracy of the $^2\Gamma_8$ level into two Kramers doublets of the tetragonal Yb^{3+} center during the phase transition. The decrease in the intensity of the high-frequency component corresponds to the decrease in the population of

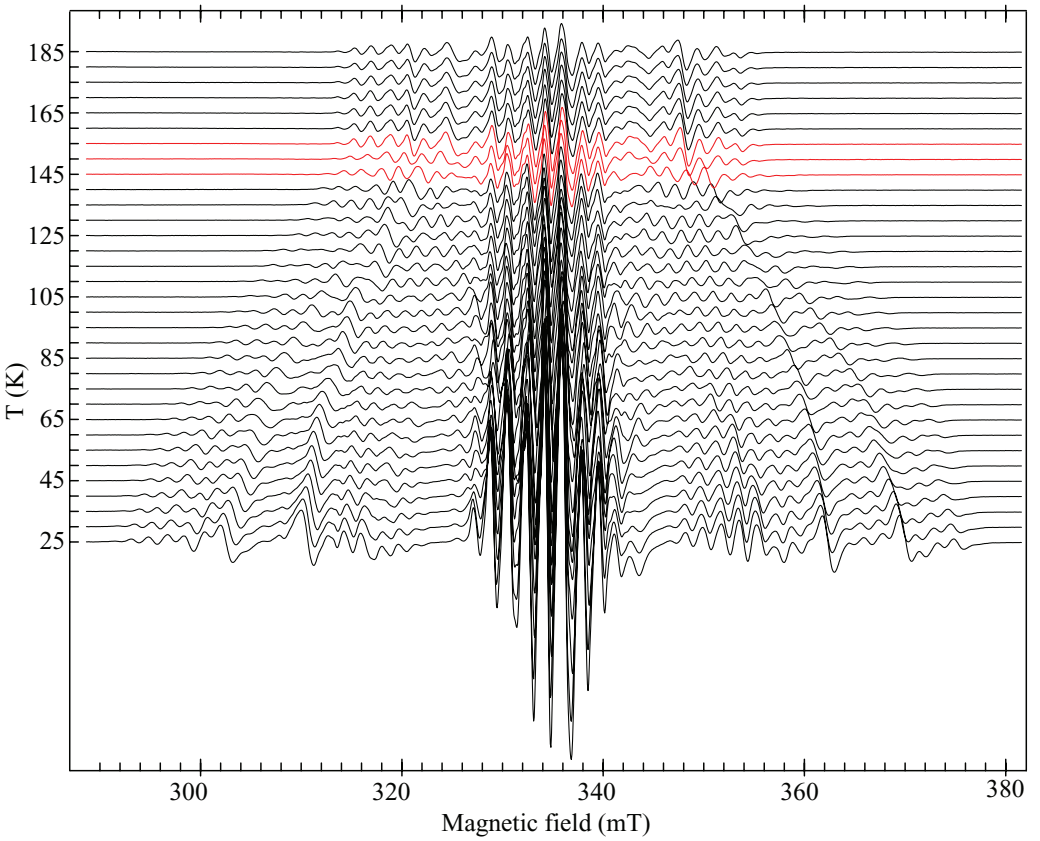

FIG. 4. (Color online) Temperature dependence of EPR spectra of the "growth" center in the Rb_2NaYF_6 crystal (sample I) for H ∥ [100] and $\nu = 9360.7$ MHz. The red lines are the phase transition region.

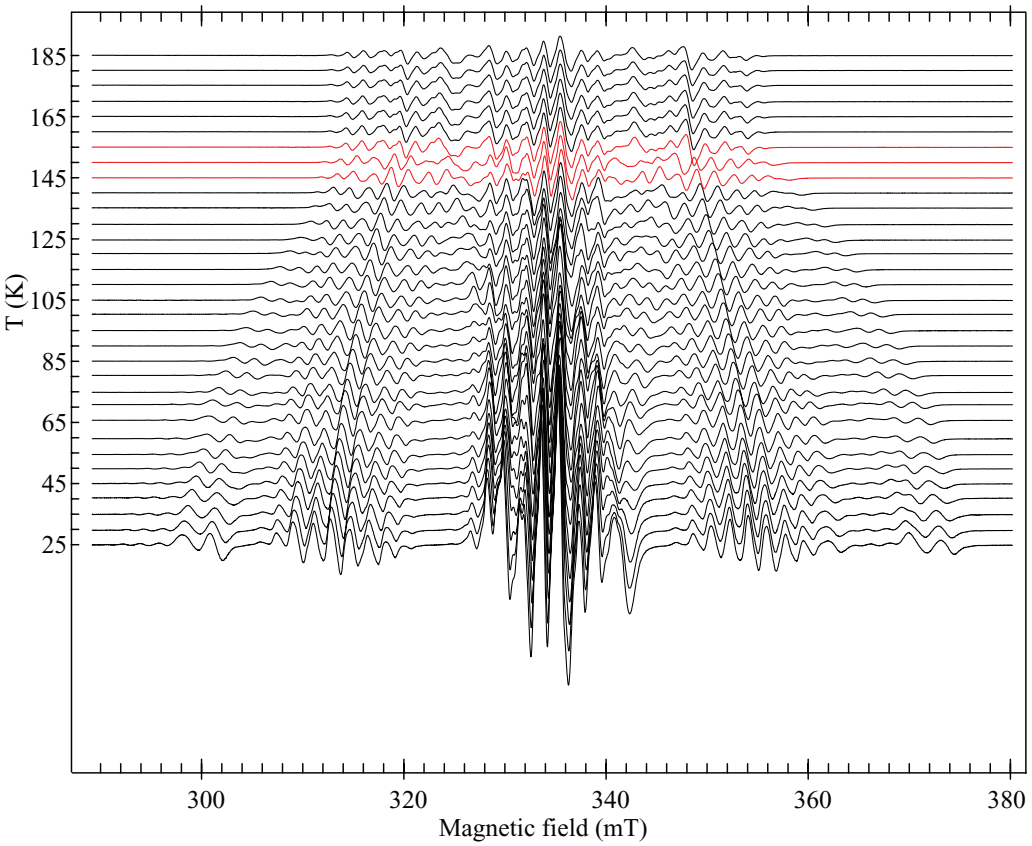

FIG. 6. (Color online) Temperature dependence of EPR spectra of the "growth" center in the "pure" Rb_2NaYF_6 crystal (sample II) for H ∥ [100] and $\nu = 9360.7$ MHz. The red lines are the phase transition region.

the ${}^3\Gamma_{t7}$ level with decreasing temperature. The line in the excitation spectrum at $T = 160$ K, which corresponds to the $\Gamma_6 \rightarrow {}^2\Gamma_7$ transition, is not observed, similarly as for Yb^{3+} in Cs_2NaYF_6.[12] This transition is forbidden by the selection rules for Yb^{3+} (T_c) for magnetic dipole and electric dipole

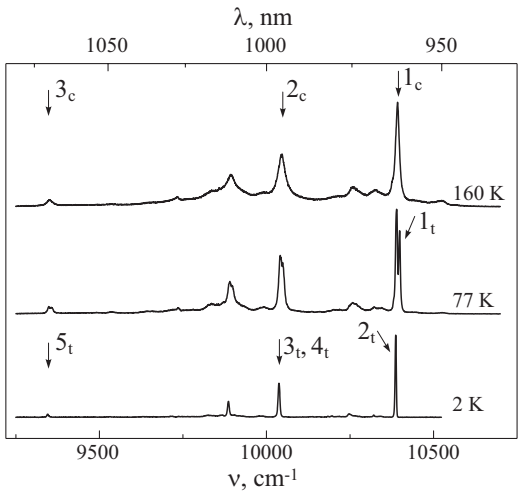

FIG. 7. Luminescence spectra of Yb^{3+} in the Rb_2NaYF_6 crystal at the temperatures of 2, 77, and 160 K. Arrows show the zero-phonon transitions of Yb^{3+}. Notations correspond to the energy level diagram in Fig. 8.

transitions. The ${}^1\Gamma_{t6} \rightarrow {}^4\Gamma_{t7}$ transition for T_{tet} is not observed as well. This is apparently due to the low probability of this transition. The positions of the ${}^2\Gamma_{t6}$ and ${}^1\Gamma_{t7}$ energy levels were established only below 10 K. This is due to the small separation between these levels (2.8 cm^{-1}). On the one hand, at higher temperatures the ${}^3\Gamma_{t6} \rightarrow {}^2\Gamma_{t6}$ (3_t) and ${}^3\Gamma_{t6} \rightarrow {}^1\Gamma_{t7}$ (4_t) transitions are not resolved because of the luminescence lines broadening. On the other hand, the population of the ${}^3\Gamma_{t7}$ level increases with temperature and the lines corresponding to the transitions ${}^3\Gamma_{t7} \rightarrow {}^2\Gamma_{t6}$ and ${}^1\Gamma_{t7}$ levels are superimposed on the luminescence lines of the ${}^3\Gamma_{t6} \rightarrow {}^2\Gamma_{t6}$ (3_t) and ${}^3\Gamma_{t6} \rightarrow {}^1\Gamma_{t7}$ (4_t) transitions. Thus the most complete set of the energy levels for Yb^{3+} (T_{tet}) was obtained in the temperature range 2–18 K. The positions of the ${}^3\Gamma_{t6}$ and ${}^3\Gamma_{t7}$ levels do not change within experimental error [see Fig. 8(a), luminescence spectra at $T = 4.2$ and 18 K]. Therefore it is reasonable to assume that the positions of the ${}^2\Gamma_{t6}$ and ${}^1\Gamma_{t7}$ levels in this temperature range do not change as well. The lines corresponding to the ${}^3\Gamma_{t6} \rightarrow {}^2\Gamma_{t6}$ (3_t) and ${}^3\Gamma_{t6} \rightarrow {}^2\Gamma_{t7}$ (5_t) transitions were chosen analogously to those for Yb^{3+} in Cs_2NaYF_6.[12] More detailed studies by high-resolution spectroscopy methods could be helpful for the more accurate determination of the optical lines positions, corresponding to the ${}^3\Gamma_{t6} \rightarrow {}^2\Gamma_{t6}$ and ${}^3\Gamma_{t6} \rightarrow {}^1\Gamma_{t7}$ transitions. Lowering of the symmetry during the phase transition also leads to the change of the electronic-vibrational spectra due to the ${}^2\Gamma_8 \rightarrow \Gamma_6$ transition for Yb^{3+} (T_c) and ${}^3\Gamma_{t7} \rightarrow {}^1\Gamma_{t6}$, ${}^3\Gamma_{t6} \rightarrow {}^1\Gamma_{t6}$ transitions for Yb^{3+} (T_{tet}) (see Fig. 9).

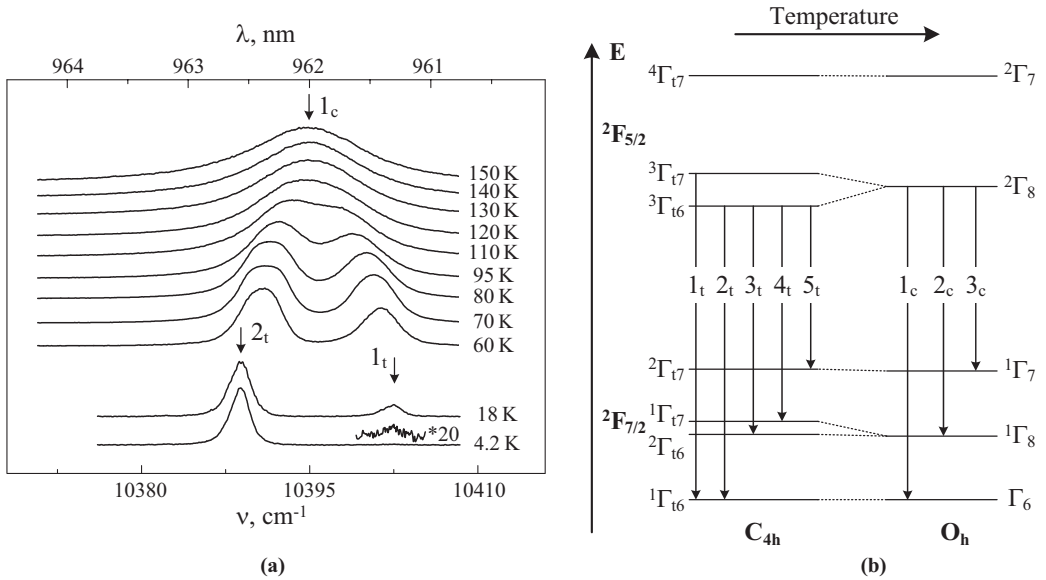

FIG. 8. Fragments of luminescence spectra of Yb^{3+} in the Rb_2NaYF_6 crystal at the temperatures of 4.2–150 K (a) and the energy level diagram of Yb^{3+} in the cubic and tetragonal crystal fields (b).

III. DISCUSSION

The above vibration structure of the optical spectra makes it possible to ascertain that the studied transition is, indeed, connected with the lattice instability pertaining to the rotations of the octahedral YF_6 ions due to the condensation of the phonon mode. Up to now, the condensation of soft modes has been experimentally observed mainly in bromine-, chlorine-, and oxygen-containing elpasolitas. As to the fluorine-containing elpasolites, for the first time, the condensation of soft modes below the transition point from the cubic to the tetragonal and then to the monoclinic phase was observed in the Raman scattering spectra of the Rb_2KScF_6 crystal in Ref. 42. It follows from the fragments of the vibration structure of the luminescence spectra (see Fig. 9) that the vibration satellite of the $^2\Gamma_8 \rightarrow {}^1\Gamma_6$ line at $T = 160$ K apparently corresponds to the soft phonon mode of the energy of 66 cm^{-1} of the cubic crystal phase that condensates during the phase transition. In the tetragonal phase ($T = 77$ K), two vibrations with the properties of the A_g and E_g symmetries at the energies of 39 and 68 cm^{-1} appear at the electron $^3\Gamma_{t6} \rightarrow {}^1\Gamma_{t6}$ line, respectively, instead of this line. They are probably hard modes, since no following phase transitions from the tetragonal phase were observed. It is also possible to assume that the electronic-vibrational mode of the energy of 178 cm^{-1} in the high-temperature spectrum is split into two vibrations with the energies of 174 and 185 cm^{-1} during the phase transition. The above considerations quantitatively agree with the results of the theoretical calculations of the lattice dynamics of the isomorphous Rb_2KScF_6 crystal.[43]

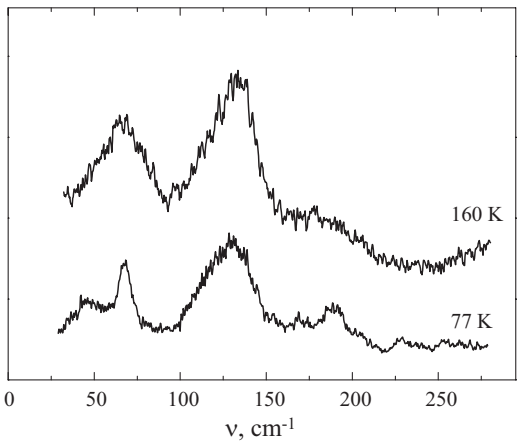

FIG. 9. Fragments of the electron-vibration luminescence spectra of Yb^{3+} in the Rb_2NaYF_6 crystal at the temperatures of 77 and 160 K. Zero on the frequency scale is the $^2\Gamma_8 \rightarrow \Gamma_6$ transition frequency at the temperature of 160 K and the $^3\Gamma_{t7} \rightarrow {}^1\Gamma_{t6}$ transition frequency at the temperature of 77 K.

A. Determination of the CF parameters

The positions of the energy levels found from the optical spectra along with the measured values of the g factors (see Table II) make it possible to determine the CF parameters acting on the Yb^{3+} ion in the cubic and tetragonal phases in Rb_2NaYF_6: Yb^{3+}. The cubic CF splits the upper $^2F_{5/2}$ multiplet of the Yb^{3+} ion into two levels Γ_7 and Γ_8 (O_h). As it follows from the spectrum of the tetragonal phase, the Γ_8 quartet is below Γ_7. The main $^2F_{7/2}$ multiplet is split into three levels Γ_7, Γ_8, and Γ_6 by the cubic CF. The measured g factor indicates that the Γ_6 doublet is the lowest, whereas it follows from the optical spectra that the Γ_8 quartet is in the center. The interaction of the Yb^{3+} ion with the cubic CF is described by the Hamiltonian of the form

$$H_{cr}(O_h) = B_4^0\left(O_4^0 + 5O_4^4\right) + B_6^0\left(O_6^0 - 21O_6^4\right), \qquad (1)$$

where CF parameters $B_k^q \equiv A_k^q\langle r^k\rangle$ incorporate the relevant radial $\langle r^k\rangle$ and $O_k^q = \sum_i O_k^q(\theta_i, \varphi_i)$ are the extended Stevens operators (ESO) depending on polar coordinates θ_i, φ_i of ith electron.[44] The radius vectors of $4f$ electrons refer to the cubic crystal axes (see Fig. 10). In the studied problem, we cannot

TABLE II. Energy levels (in cm^{-1}) and g factors of ion Yb^{3+} in Rb_2NaYF_6.

Cubic phase			Tetragonal phase			
$T = 160$ K			$T = 2$–18 K			
Irrep and g factor	Exp.	Theory	J	Irrep and g factor	Exp.	Theory
$^2\Gamma_7$	. . .	11142.6 (8)	$^2F_{5/2}$	$^4\Gamma_{t7}$	. . .	11143.5 (1)
$^2\Gamma_8$	10395.0 (4)	10395. (8)		$^3\Gamma_{t7}$	10402.3 (1)	10402.3 (1)
				$^3\Gamma_{t6}$	10388.8 (1)	10388.8 (1)
$^1\Gamma_7$	1041.0 (8)	1041 (1.6)	$^2F_{7/2}$	$^2\Gamma_{t7}$	1041.4 (5)	1041.4 (2)
$^1\Gamma_8$	348.0 (8)	348 (1.6)		$^1\Gamma_{t7}$	350.6 (3)	350.6 (2)
				$^2\Gamma_{t6}$	347.8 (3)	347.8 (1)
Γ_6	0	0		$^1\Gamma_{t6}$	0	0
g (Γ_6)	[a]	−2.667		g ($^1\Gamma_{t6}$)	| 2.788 |	−2.862
				g ($^1\Gamma_{t6}$)	| 2.473 |	−2.570

[a]It is impossible to determine the g factors because no EPR spectra are observed at $T > 50$ K (see text and Fig. 3).

use the ESO $O_k^q(\mathbf{J})$ within J-multiplet because we consider simultaneously $^2F_{7/2}$ and $^2F_{5/2}$ multiplets of the Yb^{3+} ion. The use of the ESO $O_k^q(\mathbf{L})$ within L multiplet is not convenient also because the necessity arises to involve the operator equivalent factors $(L\|\alpha\|L)$, $(L\|\beta\|L)$, and $(L\|\gamma\|L)$ for the ^2F multiplet of the f^{13} configuration. The notion of the ESO, i.e., the full set of operator equivalents $O_k^q(\mathbf{J})$, $O_k^q(\mathbf{L})$ has been first introduced in Ref. 45 and generalized in Ref. 46 (for a review of various operators used in EPR and optical spectroscopy, see Refs. 47 and 48). The theoretical energy levels were determined by the diagonalization of the energy matrices in which the interaction $H_{cr}(O_h)$ and the spin-orbit interaction $H_{so} = -\xi(\mathbf{SL})$, where ξ is the spin-orbit interaction parameter, $\mathbf{S}$ and $\mathbf{L}$ are the operators of the spin and orbital moments of the Yb^{3+} ion, respectively, were taken into account. The operators O_k^q in Hamiltonian (1) were expressed in Racah's unit orbital tensor operators, the matrix elements of which were calculated with the use of Wigner-Eckart theorem.[49] The 3-j and 6-j symbols were taken from the tables given in Ref. 50. The wave functions of the low-lying Kramers doublet were used to calculate the g factor. The diagonal in the J matrix elements of the Zeeman Hamiltonian $H_z = \beta\mathbf{H}(\mathbf{L} + g_s\mathbf{S})$ were calculated with the use of the Lande g factors of multiplets ($g_{7/2} = 6/7 + g_s/7$, $g_{5/2} = 8/7 + g_s/7$), but off-diagonal elements were found with the use of Wigner-Eckart theorem with the reduced matrix element

$$(^2F_{7/2}\|L + g_s S\|^2F_{5/2}) = 4(g_s - 1)\sqrt{3/14}.$$

Then, four experimental quantities (g factor and three energy differences) were fit by means of the least-squares procedure to determine B_k^0 and ξ. The best-fit results are given in Table III (T_c- exp.).

When analyzing the optical spectra of the tetragonal centers we assume that the phase transition from the cubic to the tetragonal phase in the Rb_2NaYF_6 crystal is implemented by the same mechanism as in a series of Rb_2NaREF_6 (RE = Dy^{3+}, Ho^{3+}, Tm^{3+}),[20,22] the tolerance factor of which is $t_G > 0.915$. Phase transitions in these structures are connected with the lattice instability due to the rotations of the octahedral ReF_6 and NaF_6 groups. According to the theoretical-group analysis of the possible distortions of the elpasolite structure,[51] the phase transition $O_h^5 \rightarrow C_{4h}^5$ is connected with the soft mode, which belongs to the center of the Brillouin zone. The corresponding distortion due to the condensation of the soft phonon of $\Gamma_4^+(F_{1g})$ symmetry[20] is denoted as of the (0,0,φ) type.[51] It is a quasi-two-dimensional motion of the rigidly coupled octahedral ions, when the rotation of one octahedron around any cubic axis leads to the distortion of the whole layer of octahedra orthogonal to this axis. Rotations of the φ-type mean that octahedra in adjacent layers are tilted at the same angle φ in the opposite direction.

Thus the Yb^{3+} ion located in the center of such rotated octahedron in the tetragonal phase is subjected to the action of the tetragonal CF of the C_{4h} group, the interaction with which should be described by the Hamiltonian of the form[52]

$$H_{cr}(C_{4h}) = B_2^0O_2^0 + B_4^0O_4^0 + B_4^4O_4^4 + B_6^0O_6^0 + B_6^4O_6^4 + B_4^{-4}O_4^{-4} + B_6^{-4}O_6^{-4}. \quad (2)$$

TABLE III. The spin-orbit interaction (ξ) and CF (B_k^q) parameters (in cm^{-1}) of Yb^{3+} for the cubic and tetragonal phases of Rb_2NaYF_6; $\Delta B_k^q(\text{exp.}) = B_k^q(T_{tet}\text{-exp.}) - B_k^q(T_c\text{-exp.})$ represents the change of ΔB_k^q due to the rotation of octahedra.

Parameter	ξ	B_2^0	B_4^0	B_4^4	B_6^0	B_6^4
T_{tet}-exp.	2911.6	−11.7	320.1	1622.9	−7.3	140.5
T_{tet}-theory			320.6	1621.8	−5.9	148.0
T_c-exp.	2911.6	0	321.9	1609.5	−6.9	144.9
T_c-theory		0	321.9	1609.5	−6.9	144.9
ΔB_k^q(exp.)		−11.7	−1.8	13.4	−0.4	−4.4
Cs_2NaYF_6 (T_c-exp.)[12]	2913.0	0	313.0	1565.0	−8.5	178.5

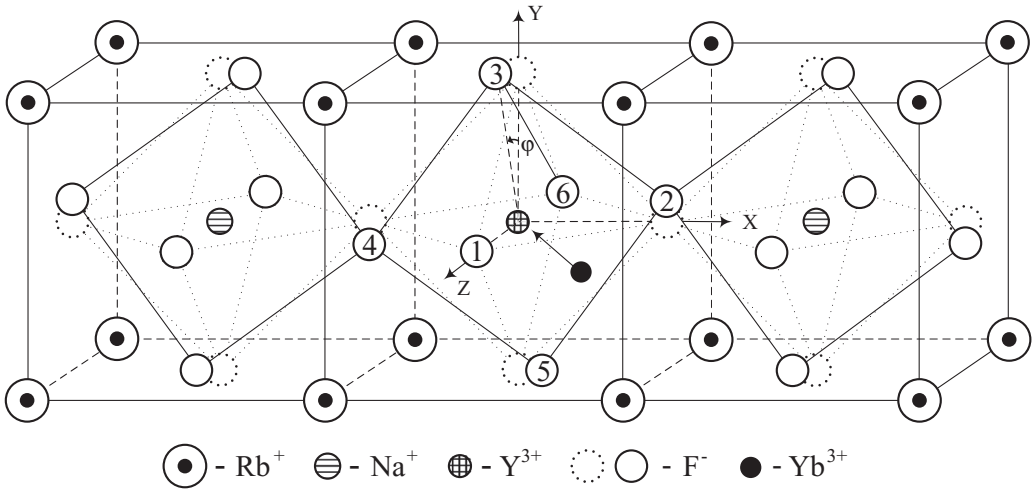

FIG. 10. Fragment of the structure of the Rb_2NaYF_6 crystal. Axes Z, X, and Y are directed along the fourfold axes of the initial cubic crystal phase. The distortion symbol of the structure is $(0,0,\varphi)$, where φ is the rotation angle of octahedra.

This Hamiltonian differs from the Hamiltonian $H_{cr}(D_{4h})$ of CF of the D_{4h} group of the higher symmetry by the two last terms $C_4^{-4}O_4^{-4}$ and $C_6^{-4}O_6^{-4}$. Therefore one may suppose that the parameters B_4^{-4} and B_6^{-4} measure directly the departure of C_{4h} from the D_{4h} symmetry. Since the effects of the descent of the cubic symmetry to the tetragonal we consider are small, we apparently may assume that the departure of C_{4h} from the D_{4h} symmetry is extremely small. Therefore, to simplify further calculations, the terms $C_4^{-4}O_4^{-4}$ and $C_6^{-4}O_6^{-4}$ in Eq. (2) are omitted. In this case, the radius vectors of $4f$ electrons in the Stevens operators of the simplified Hamiltonian (2) refer to the coordinate system with the Z axis directed along the rotation axis of the octahedron, and the X and Y axes are directed as shown in Fig. 10. For the definitions of the axis system, symmetry properties and forms of the CF Hamiltonian of the low tetragonal symmetry readers may consult Refs. 53 and 54. The values of the relevant parameters are determined in the same manner as for the cubic centers [see Table III (T_{tet}–exp.)].

B. Superposition model analysis

To estimate quantitatively the lattice distortions near an impurity ion, we use the superposition model (SM),[55–60] which postulates that the CF parameters are linear superposition of parameters due to each ligand. The resulting CF parameters are

$$B_k^q = \sum_i K_k^q(\Theta_i,\Phi_i)\bar{B}_k(R_i), \tag{3}$$

where $K_k^q(\Theta_i,\Phi_i)$ are the coordination factors depending on the angular positions (defined by the spherical angles Θ_i and Φ_i) of all ions located at the distance R_i from the impurity ion (the most complete table of their expressions is given in Ref. 61) and $\bar{B}_k(R_i)$ are the "intrinsic" parameters depending on the ligand type. The dependence of the $\bar{B}_k(R_i)$ parameters in the limited regions of distances is assumed as a power-law:

$$\bar{B}_k(R_i) = \bar{B}_k(R_0)\left(\frac{R_0}{R_i}\right)^{t_k}, \tag{4}$$

where t_k are the power-law exponents and $\bar{B}_k(R_0)$ is the intrinsic parameter of the model referring to reference distance R_0 usually taken equal to the sum of ionic radii of the magnetic ion and ligand.

The quantities t_k and $\bar{B}_k(R_0)$, which characterize the CF created by F^- ions, can be determined from the CF parameters of the cubic centers of the Yb^{3+} ion in Rb_2NaYF_6 and Cs_2NaYF_6 isomorphous crystal if the equilibrium distances R of the F^- ligands to the impurity Yb^{3+} ion are known. In this manner, we analyzed the structure of the trigonal fluorine centers of the Yb^{3+} ion in SrF_2 and BaF_2 crystals.[62] Unfortunately, such information about the distances to the nearest neighbors is not available for impurity crystals of fluoroelpasolites. Hence we first assumed R_0 equal to 0.2153 nm, i.e., the sum of ionic radii of Yb^{3+} and F^- ions.[63] Second, we determined t_4, $\bar{B}_4(R_0)$, t_6, and $\bar{B}_6(R_0)$ as follows. We assumed that the experimental parameters B_4^0 and B_6^0 (see Table III) of the cubic Yb^{3+} centers in Rb_2NaYF_6 and Cs_2NaYF_6 are determined only by the six F^- ions of the nearest environment and can be described by a single set of parameters t_k and $\bar{B}_k(R_0)$, which can be found from the following system of four equations:

$$\begin{aligned}
B_4^0(\mathrm{Rb}) &= \sum_i \bar{B}_4(R_i)K_4^0(\Theta_i,\Phi_i),\\
B_4^0(\mathrm{Cs}) &= \sum_i \bar{B}_4(R_i)K_4^0(\Theta_i,\Phi_i),\\
B_6^0(\mathrm{Rb}) &= \sum_i \bar{B}_6(R_i)K_6^0(\Theta_i,\Phi_i),\\
B_6^0(\mathrm{Cs}) &= \sum_i \bar{B}_6(R_i)K_6^0(\Theta_i,\Phi_i).
\end{aligned} \tag{5}$$

Taking into account that the coordinates of the fluorine ions 1–6, forming the octahedron around the Yb^{3+} ion (see Fig. 10), in the coordinate system of the cubic center are $R_1 = R_2 = R_3 = R_4 = R_5 = R_6 = R$, $\Theta_1 = 0$, $\Theta_2 = \Theta_3 = \Theta_4 = \Theta_5 = \pi/2$, $\Theta_6 = \pi$, $\Phi_2 = 0$, $\Phi_3 = \pi/2$, $\Phi_4 = \pi$, $\Phi_5 = 3\pi/2$, Eq. (5) can

be rewritten as

$$B_4^0(\mathrm{Rb}) = \frac{7}{2}\bar{B}_4\left(\frac{R_0}{R}\right)^{t_4}, \quad B_4^0(\mathrm{Cs}) = \frac{7}{2}\bar{B}_4\left(\frac{R_0}{R}\right)^{t_4},$$
$$B_6^0(\mathrm{Rb}) = \frac{3}{4}\bar{B}_6\left(\frac{R_0}{R}\right)^{t_6}, \quad B_6^0(\mathrm{Cs}) = \frac{3}{4}\bar{B}_6\left(\frac{R_0}{R}\right)^{t_6}, \tag{6}$$

with the simplified notation $\bar{B}_k(R_0) = \bar{B}_k$. To find reasonable values of the t_k and $\bar{B}_k$, we make some assumptions concerning the sizes of octahedra in both crystals. The Yb^{3+} ions doped in the matrix crystals in the position of Y^{3+} ions are apparently at distances from the F^- ions that are intermediate between the distances at which they are located in Rb_2NaYbF_6 and Cs_2NaYbF_6 and distances between Y^{3+} and F^- ions in Rb_2NaYF_6 and Cs_2NaYF_6. Therefore it is reasonable to assume that the distance between Yb^{3+} and F^- ions in the doped crystal cannot be less than that in Rb_2NaYbF_6 (0.2206 nm)[1] and larger than the distance between them in Cs_2NaYF_6 (0.2264 nm).[1] Using these assumptions, we solved Eq. (6) for the smallest possible ($R = 0.2206$ nm) size of octahedra. When varying the parameters, we also kept in mind that the reasonable values of t_4 and t_6, which characterize the interaction of the RE^{3+} ion with the ligand F^-, change from about 5 to 8 and 8 to 15, respectively.[55–57] Hence we obtained $\bar{B}_4 = 103.72\ \mathrm{cm}^{-1}$, $t_4 = 5.516$, $\bar{B}_6 = -14.12\ \mathrm{cm}^{-1}$, and $t_6 = 13.098$. Then using these values as initial ones, we solved a system of only two equations:

$$B_4^0 = \frac{7}{2}\bar{B}_4\left(\frac{R_0}{R}\right)^{t_4}, \quad B_6^0 = \frac{3}{4}\bar{B}_6\left(\frac{R_0}{R}\right)^{t_6}, \tag{7}$$

in order to find, for Rb_2NaYF_6, Yb^{3+} the model parameters and the octahedron size R, with which the experimental values of the CF parameters of the cubic center would be best described. We also set the octahedron size to be less than that in Rb_2NaYF_6 and larger than that in Rb_2NaYbF_6. One set was $\bar{B}_4 = 110.09\ \mathrm{cm}^{-1}$, $t_4 = 6.46$, $\bar{B}_6 = -12.56\ \mathrm{cm}^{-1}$, $t_6 = 11.19$, and $R = 0.2214$ nm. For these model parameters, the CF parameters of the cubic centers were $B_4^0 = 321.90\ \mathrm{cm}^{-1}$ and $B_6^0 = -6.90\ \mathrm{cm}^{-1}$, which agrees with the experimental values (see Table III T_c-theory). The quantity R was 0.2214 nm, i.e., the observed CF parameters require that the octahedron in Rb_2NaYbF_6 is somewhat elongated.

C. Structure of tetragonal centers

When analyzing the structure of tetragonal centers, we suppose that the Yb^{3+} ion and four F_2, F_3, F_4, and F_5 ions remain in the same plane perpendicular to the axis of the center when the octahedron rotates and that their distances to the impurity ion remain equal to each other due to the tetragonal symmetry of the center. In the tetragonal crystal phase, the rotated octahedron can be either elongated or compressed, therefore we assume $R_2 = R_3 = R_4 = R_5$. The distances from the fluorine F_1 and F_6 ions located on the rotation axis also remain equal: $R_1 = R_6$, but during the deformation of the octahedron they will change to R_1'. The angular coordinates $\Theta_1 = 0$, $\Theta_2 = \Theta_3 = \Theta_4 = \Theta_5 = \pi/2$, $\Theta_6 = \pi$, of all ions do not change. Only the azimuthal angles change as $\Phi_2 = \varphi$, $\Phi_3 = \pi/2 + \varphi$, $\Phi_4 = \pi + \varphi$, $\Phi_5 = 3\pi/2 + \varphi$, where φ is the rotation angle of the octahedron. Thus the CF parameters B_4^4 and B_6^4 in the tetragonal phase depend on φ, and are determined as

$$\begin{aligned} B_4^4 &= \frac{35}{2}\bar{B}_4(R_2)(1 + 4\cos^4\varphi - 4\cos^2\varphi \\ &\quad + 4\sin^4\varphi - 4\sin^2\varphi), \\ B_6^4 &= -\frac{63}{4}\bar{B}_6(R_2)(1 + 4\cos^4\varphi - 4\cos^2\varphi \\ &\quad + 4\sin^4\varphi - 4\sin^2\varphi). \end{aligned} \tag{8}$$

Since the rotation angle is small, one expands the functions in a series in the vicinity of $\varphi = 0$, then with accuracy of up to the fourth powers in φ, these parameters are

$$B_4^4 = \frac{35}{2}\bar{B}_4(R_2)\left(1 - 8\varphi^2 + \frac{32}{3}\varphi^4\right),$$
$$B_6^4 = -\frac{63}{4}\bar{B}_6(R_2)\left(1 - 8\varphi^2 + \frac{32}{3}\varphi^4\right). \tag{9}$$

Then the changes of the CF parameters $\Delta B_k^q(\mathrm{theory}) = B_k^q(T_{\mathrm{tet}}\text{−theory}) - B_k^q(T_c\text{−theory})$, due to the rotation of octahedra are described as

$$\begin{aligned} \Delta B_4^0 &= 2\bar{B}_4(R_1') + \frac{3}{2}\bar{B}_4(R_2) - \frac{7}{2}\bar{B}_4(R), \\ \Delta B_4^4 &= \frac{35}{2}\bar{B}_4(R_2)\left(1 - 8\varphi^2 + \frac{32}{3}\varphi^4\right) - \frac{35}{2}\bar{B}_4(R), \\ \Delta B_6^0 &= 2\bar{B}_6(R_1') - \frac{5}{4}\bar{B}_6(R_2) - \frac{3}{4}\bar{B}_6(R), \\ \Delta B_6^4 &= -\frac{63}{4}\bar{B}_6(R_2)\left(1 - 8\varphi^2 + \frac{32}{3}\varphi^4\right) + \frac{63}{4}\bar{B}_6(R). \end{aligned} \tag{10}$$

From Eq. (10) using the values $\Delta B_k^q(\mathrm{exp.})$ from Table III, one can determine the distances R_1' and R_2, characterizing the octahedron structure and the rotation angle φ. The self-consistent solution of Eq. (10) leads to $R_1' = 0.2221$ nm, $R_2 = 0.2207$ nm, and the angle $\varphi = 2.1^\circ$. In this tetragonal center, the F_1 and F_6 ions move away from the paramagnetic ion by 0.0007 nm and four planar ions, in contrary, approach it by 0.0014 nm. Thus, during the transition into the tetragonal phase, the rotated octahedron is elongated along the rotation axis by about 0.0014 nm and compressed in the direction perpendicular to the axis by about 0.0028 nm. With these R_1' and R_2 and φ values, all CF parameters are obtained with correct signs and are quantitatively described rather well (see Table II T_{tet}–theory). For example, the value $B_4^0(T_{\mathrm{tet}}\text{−theory})$ differs from $B_4^0(T_{\mathrm{tet}}\text{−exp.})$ only by 0.5 cm^{-1}. The largest deviation $B_6^4(T_{\mathrm{tet}}\text{−theory}) - B_6^4(T_{\mathrm{tet}}\text{−exp.}) = 7.5\ \mathrm{cm}^{-1}$ is found for B_6^4, although the experimental parameter is not very large $B_6^4(T_{\mathrm{tet}}\text{−exp.}) = 140.5\ \mathrm{cm}^{-1}$. It should be noted that the predicted distortions of octahedra are similar to those established for the analogous phase transition in the isomorphous Rb_2NaHoF_6 crystal by x rays.[17]

IV. CONCLUSION

We have presented an evidence of the observation of the structural phase transition in the Rb_2NaYF_6 crystal by EPR and optical spectroscopy. We also determined the rotation angle of LnF_6 octahedra from the CF parameters. The above results

demonstrate that the distorted tetragonal structure of the initial cubic phase of the Rb_2NaYF_6 crystal cannot be described only by the critical order parameter, i.e., by rotation of octahedra but also by noncritical displacements of atoms in the rotated fluorine octahedra.

ACKNOWLEDGMENTS

This study was supported by the grant NSh-5602-2012.2 and the Russian Foundation for Basic Research (Project No. 13-02-97031r_Volga region_a).

[1] S. Aleonard and C. Pouzet, J. Appl. Crystallogr. **1**, 113 (1968).
[2] G. Meyer, Prog. Solid State Chem. **14**, 141 (1982).
[3] D. Babel and A. Tressaud in *Inorganic Solid Fluorides, Chemistry and Physics*, edited by P. Hagenmuller (Academic Press, New York, 1985), p. 77.
[4] E. Bucher, H. J. Guggenheim, K. Andres, G. W. Hull, Jr., and A. S. Cooper, Phys. Rev. B **10**, 2945 (1974).
[5] P. A. Tanner, M. Chua, and M. F. Reid, J. Alloys Compounds **225**, 20 (1995).
[6] F. S. Richardson, M. F. Reid, J. Dallara, and R. D. Smith, J. Chem. Phys. **83**, 3813 (1985).
[7] M. F. Reid and F. S. Richardson, J. Chem. Phys. **83**, 3831 (1985).
[8] P. Tanner, Mol. Phys. **58**, 317 (1986).
[9] P. A. Tanner, V. V. R. K. Kumar, C. K. Jayasankar, and M. F. Reid, J. Alloys Compounds **215**, 349 (1994).
[10] P. A. Tanner, L. Ning, V. N. Makhov, N. M. Khaidukov, and M. Kirm, J. Phys. Chem. B **110**, 12113 (2006).
[11] X. Zhou, M. F. Reid, M. D. Faucher, and P. A. Tanner, J. Phys. Chem. B **110**, 14939 (2006).
[12] M. L. Falin, K. I. Gerasimov, A. M. Leushin, and N. M. Khaidukov, J. Lumin. **128**, 1103 (2008).
[13] P. A. Tanner, M. D. Faucher, and X. Zhou, J. Phys. Chem. A **115**, 2557 (2011).
[14] K. S. Aleksandrov and B. V. Beznosikov, *Perovskitopodobnyekristally* (Nauka, Novosibirsk, 1997) (in Russian).
[15] B. I. Swanson, B. C. Lucas, and R. R. Ryan, J. Chem. Phys. **69**, 4328 (1978).
[16] E. J. Veenendaal, H. B. Brom, and J. Ihringer, Physica B **114**, 31 (1982).
[17] J. Ihringer, Acta Crystallogr. A **36**, 89 (1980).
[18] A. Gormezano and M. T. Weller, J. Mater. Chem. **3**, 979 (1993).
[19] T. Nakajima and H. Suzuki, J. Low Temp. Phys. **96**, 47 (1994).
[20] P. Selgert, C. Lingner, and B. Luthi, Z. Phys. B **55**, 219 (1984).
[21] K. S. Aleksandrov, S. V. Misyul, M. S. Molokeev, and V. N. Voronov, Phys. Solid State **51**, 2359 (2009).
[22] J. Ihringer, Solid State Commun. **41**, 525 (1982).
[23] A. V. Egorov, L. D. Livanova, M. S. Tagirov, and M. A. Teplov, Phys. Solid. State **22**, 2836 (1980).
[24] E. J. Veenendaal and H. B. Brom, Physica B **113**, 118 (1982).
[25] J. M. Dance, J. Grannec, A. Tressaud, and M. Moreno, Phys. Status Solidi B **173**, 579 (1992).
[26] S. Khairoun, A. Tressaud, J. Grannec, J. M. Dance, and A. Yacoubi, Phase Transitions **13**, 157 (1988).
[27] I. N. Flerov, M. V. Gorev, and V. N. Voronov, Phys. Solid State **38**, 396 (1996).
[28] M. Couzi, S. Khairoun, and A. Tressaud, Phys. Status Solidi A **98**, 423 (1986).
[29] M. V. Gorev, I. N. Flerov, V. N. Voronov, and S. V. Misyul, Phys. Solid State **35**, 1022 (1993).
[30] I. N. Flerov, M. V. Gorev, A. Tressaud, and J. Grannec, Ferroelectrics **217**, 21 (1998).
[31] I. N. Flerov, M. V. Gorev, K. S. Aleksandrov, A. Tressaud, J. Grannec, and M. Couzi, Mater. Sci. Eng. R **24**, 81 (1998).
[32] E. G. Maksimov, V. I. Zinenko, and N. G. Zamkova, Phys. Usp. **174**, 1145 (2004).
[33] A. Tressaud, S. Khairoud, J. P. Chaminade, and M. Couzi, Phys. Status Solidi A **98**, 417 (1986).
[34] H. Guengard *et al.*, C. R. Acad. Sci. Ser. 2 **317**, 37 (1993).
[35] B. D. Dunlap, G. R. Davidson, M. Eibschutz, H. J. Guggnheim, and R. C. Sherwood, and J. Physiqie, Colloque C6 **35**, 429 (1974).
[36] C. K. Duan, P. A. Tanner, V. Babin, and A. Meijerink, J. Chem. Phys. C **113**, 12580 (2009).
[37] B. F. Aull and H. P. Jenssen, Phys. Rev. B **34**, 6647 (1986).
[38] V. A. Latypov and M. L. Falin, Prib. Tekh. Eksp. **4**, 164 (2001).
[39] M. L. Falin, K. I. Gerasimov, B. N. Kazakov, and M. A. Yakshin, Appl. Magn. Res. **17**, 103 (1999).
[40] M. L. Falin, V. A. Latypov, H. Bill, and D. Lovy, Appl. Magn. Res. **14**, 427 (1998).
[41] M. L. Falin, O. A. Anikeenok, V. A. Latypov, N. M. Khaidukov, F. Callens, H. Vrielinck, and A. Hoefstaetter, Phys. Rev. B **80**, 174110 (2009).
[42] A. N. Vtyurin, A. Bulou, A. S. Krylov, and V. N. Voronov, Phys. Solid State **43**, 2154 (2001).
[43] V. I. Zinenko and N. G. Zamkova, Phys. Solid State **41**, 1297 (1999).
[44] Y. Y. Yeung and C. Rudowicz, Computers Chem. **16**, 207 (1992).
[45] C. Rudowicz, J. Phys. C **18**, 1415 (1985); **19**, 3837 (1985).
[46] C. Rudowicz and C. Y. Chung, J. Phys.: Condens. Matter **16**, 5825 (2004).
[47] C. Rudowicz, Magn. Res. Rev. **13**, 1 (1987); **13**, 335 (1988).
[48] C. Rudowicz and S. K. Misra, Appl. Spectrosc. Rev. **36**, 11 (2001).
[49] B. R. Judd, *Operator Techniques in Atomic Spectroscopy* (McGraw-Hill, New-York, 1963).
[50] M. Rotenberg, N. Metropolis, R. Biwins, and J. K. Wooten, Jr, *The 3- and 6-j Symbols* (Mass. Tech. Press, Cambridge, 1959).
[51] K. S. Aleksandrov and S. V. Misyul, Sov. Phys. Crystallogr. **26**, 612 (1981).
[52] A. M. Leushin, *Tables of Functions Transforming According to the Irreducible Representations of Crystal Point Groups* (Nauka, Moscow, 1968) (in Russian).
[53] C. Rudowicz, Chem. Phys. **97**, 43 (1985).
[54] C. Rudowicz, P. Gnutek, and M. Karbowiak, Opt. Mater. **33**, 1557 (2011).
[55] D. J. Newman, Adv. Phys. **20**, 197 (1971).
[56] D. J. Newman, Aust. J. Phys. **31**, 79 (1978).

[57]D. J. Newman and B. Ng, Rep. Progr. Phys. **52**, 699 (1989).
[58]D. J. Newman and B. Ng, *Superposition model*, in Crystal Field Handbook, edited by D. J. Newman and B. Ng (Cambridge University Press, Cambridge, 2000), pp. 83–119.
[59]M. Andrut, M. Wildner, and C. Rudowicz, EMU Notes Mineralogy **6**, 145 (2004).
[60]M. Karbowiak, C. Rudowicz, and P. Gnutek, Opt. Mat. **33**, 1147 (2011).
[61]C. Rudowicz, J. Phys. C **20**, 6033 (1987).
[62]M. L. Falin, K. I. Gerasimov, V. A. Latypov, and A. M. Leushin, J. Phys: Condens. Matter **15**, 2833 (2003).
[63]R. D. Shannon, Acta Crystallogr. A **32**, 751 (1976).